International Forum on Aeroelasticity and Structural Dynamics
IFASD-2017
25-28 June 2017, Como - Italy

NESTED LIMIT CYCLES IN TRANSONIC FLUTTER

Oddvar O. Bendiksen

Mechanical and Aerospace Engineering Department
University of California, Los Angeles
Los Angeles, CA 90095-1597, USA
e-mail: oddvar@seas.ucla.edu

Keywords: Nonlinear Transonic Flutter, Multiple Limit Cycles.

Abstract: Multiple or nested limit cycle oscillations (LCOs) were first observed in wind tunnel tests of an unswept supercritical wing in transonic flow, restricted by the supports to two degrees of freedom (pitch and plunge). In this case the flow was essentially two-dimensional, and the coexistence of two LCOs of different amplitudes can be explained in terms of the transition from Tijdeman Type A to Type B shock motion, which limits the energy flow from the fluid to the structure. For a highly nonsymmetrical wing, the transitions on the upper and lower surfaces will occur at different amplitudes, resulting in nested limit cycles. Recent computational results suggest that nested limit cycles should occur for most transonic wings, if the wings exhibit LCO-type flutter near Mach 1. In this paper, results are presented for flutter cases where 3 nested limit cycles are present in the transonic region. Possible physical mechanisms responsible for multiple LCOs are discussed, as are the computational and experimental implications. Calculations indicate that at some Mach numbers one or more of the nested LCOs may become unstable and eventually disappear by "morphing" into neighboring LCOs. The outer LCO is also susceptible to amplitude instabilities and may gradually transition into strong flutter. In a wind tunnel or flight test this could be dangerous, because a small change in Mach number or dynamic pressure could transform a benign LCO into hard flutter. These observations also have important computational implications in code verification and validation.

1 INTRODUCTION

Wind tunnel flutter tests at DLR in Göttingen [1-2] of a "two-dimensional" wing with an NLR 7301 supercritical airfoil have demonstrated that transonic limit cycle flutter can and does occur even in the absence of noticeable flow separation or structural nonlinearities. These flutter tests have also shown that complex and highly nonlinear flutter behaviors appear even at relatively small flutter amplitudes. An intriguing result was the discovery of two "nested" LCOs, with different amplitudes, coexisting at the same Mach number and angle of attack, Fig. 1. It was observed that a transition from the "lower" to the "upper" LCO (and vice versa) could be accomplished by applying relatively small force perturbations in the plunge direction, either in-phase or out-of-phase with the plunge velocity at the elastic axis, thus providing short bursts of negative or positive structural damping.

The fundamental physical mechanism behind the observed multiple limit cycles cannot be attributed to viscous effects, because the LCOs also show up in Euler-based calculations. It was concluded in Ref. 3 that the lower (upper) LCO is caused by the shock motion on the lower (upper) surface of the wing undergoing a transition from Tijdeman Type A (continuous) to Type B (intermittent) motion, which results in a rapid decrease in the aerodynamic work on the wing. For wings with highly nonsymmetrical sections, such as the supercritical NLR 7301 wing, two nested limit cycles of different amplitudes should occur, since the Type A to B shock transitions will occur at different amplitudes on the upper and lower surfaces.

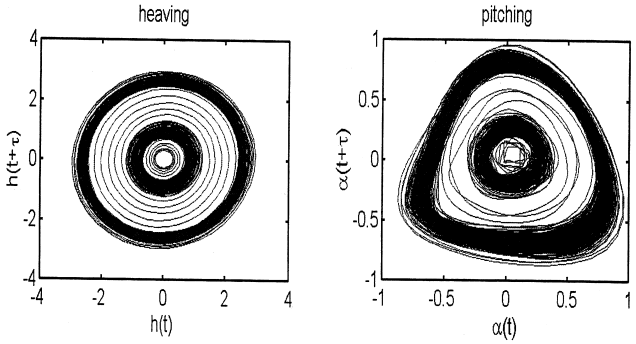

Figure 1: Multiple (nested) limit cycles observed during flutter test of an NLR 7301 wing model at DLR [1].

Similar low-amplitude transonic limit cycle flutter was later observed during wind tunnel tests at DLR of a high-aspect-ratio swept wing [4]. Because the LCO-type flutter was encountered at an angle of attack and lift coefficient close to design, it cannot be classified as stall flutter, nor is it evident from the experimental data that trailing edge separation played a significant role. Based on calculations on similar a generic transport wing (the G-Wing), we have concluded that the LCO-type transonic flutter observed on the Göttingen wing should also be expected for other swept wings of high aspect ratio and similar flexibility [5]. Surprisingly, the G-Wing also has two nested LCOs over a range of transonic Mach numbers. Although no evidence of multiple LCOs was reported in the wind tunnel tests of the similar Göttingen wing, it should be noted that special initial conditions would be necessary to discover the outer LCO. Unless a sufficiently large initial disturbance is provided, the aeroelastic response will gravitate to the lower-amplitude inner LCO.

To our knowledge, no previous theoretical or experimental investigations have found more than two limit cycles at the same Mach number [6]. We have recently discovered several such cases, where 3 nested limit cycles are present at transonic Mach numbers. The main objectives of this study are to (1) investigate the physical mechanism(s) responsible for the appearance of multiple nested limit cycles of wings at transonic conditions; (2) to identify the main parameters affecting the qualitative and quantitative aeroelastic behaviors; and (3) to consider the theoretical and experimental implications of our findings.

2 FLUTTER NEAR MACH 1

2.1 Mixed subsonic-supersonic flows

Transonic flow over aircraft wings is inherently nonlinear, even in the limit of small disturbances. By inherently nonlinear, we mean that there is no uniformly valid linear first-order equation for steady or unsteady transonic flows. Two types of nonuniformities occur: nonuniformities with respect to a parameter, such as the Mach number, and nonuniformities with respect to the coordinates (time and space). By nonuniformities in this context we mean a mathematical breakdown of the solution for certain values of a parameter, or for certain regions of space-time.

There is a fundamental difference between the supersonic region(s) in transonic flow and linearized supersonic flow. In linear supersonic flow, the characteristics (Mach waves) are straight lines with a constant slope, and only one set of characteristics is allowed on the upper or lower airfoil surface, in order to satisfy the radiation condition; i.e., disturbances must propagate away from the wing in the far field. In the transonic case, Fig. 2, both families of characteristics are present in the supersonic pocket(s), one set representing expansion waves and the other compression waves. The slopes of the characteristics change as one moves away from the airfoil surface and become vertical at the sonic line. From this behavior and the fact that the spatial extent of the local supersonic or subsonic region is not known but must be determined as part of the solution, it is clear that linear equations cannot describe the physics of a mixed flow.

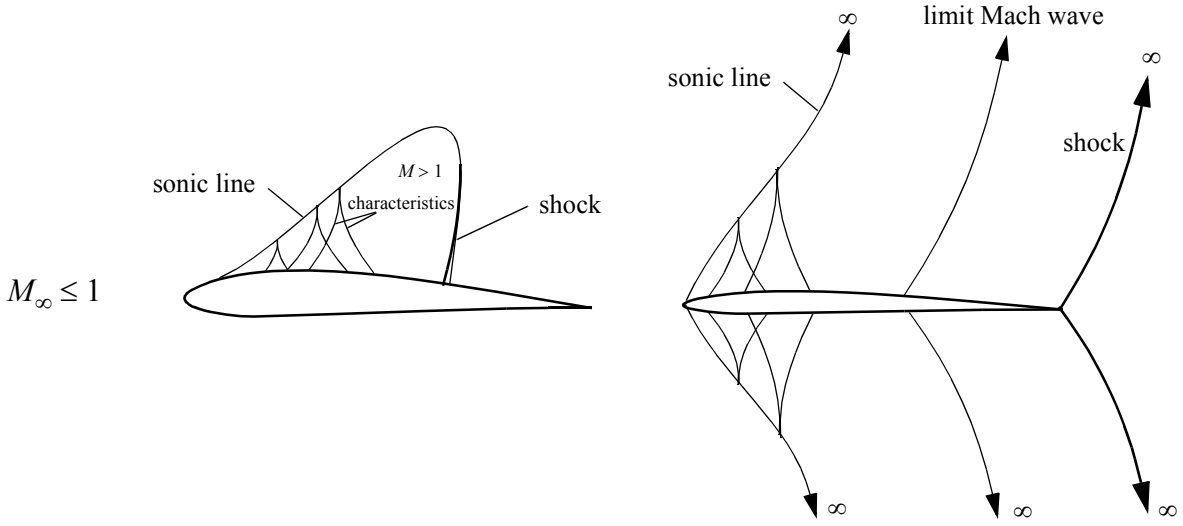

a) Transonic flow with $M_{cr} < M_\infty < 1$.

b) Sonic flow ($M_\infty = 1$).

Figure 2: Comparison of flow regions in transonic flows for $M_{cr} < M_\infty \le 1$ (2D inviscid case).

2.2 Mach number freeze

The Mach number freeze is brought about by a nonuniformity in the aerodynamic solution at infinity. It is a direct consequence of the fundamental change that must occur in the far field as the Mach number passes through one, and not by any near-field changes around the wing. Consequently, it is only weakly influenced by changes in the local flow caused, for example, by shock-boundary layer interactions and flow separation behind the shocks.

In a sonic flow ($M_\infty = 1$), Fig. 2b), the supersonic regions extend to infinity, as do the sonic lines and the trailing-edge shocks. A limit Mach wave (characteristic) appears on the upper and lower surfaces, which is asymptotic to the sonic line at infinity. These Mach waves divide the flow-field into two regions: an upstream region that can influence the upstream flow, and a downstream region that can not. Because the flow-field behind the limit Mach waves cannot influence the flow in front of these waves, it is similar to a supersonic flow-field. From this it follows that the far field must change, from a dominant vortex (circulatory) term fixed by the lift on the wing, to a source-like far field without circulatory terms; see Cole [7].

As long as $M_\infty < 1$, the far field is subsonic and the dominant term is a vortex term given by the lift. At Mach 1, this far field disappears and is replaced by a similarity form corresponding to $M_\infty = 1$ [8]. If we model the flow as a small perturbation about the perfectly sonic flow, a nonuniformity at infinity will appear. Near to the wing or body, on the other hand, the solution is valid and from it one can deduce the important *law of stabilization* or *Mach number freeze*,

$$\left.\frac{dM}{dM_\infty}\right|_{M_\infty = 1} = 0 \tag{1}$$

which has important implications in aeroelastic problems.

The practical importance of the Mach number freeze in an aeroelastic setting arises from the fact that the flow near the airfoil ahead of the shock(s) can be considered a small perturbation of a sonic flow. Because the local Mach number freezes, the pressure on the airfoil surface ahead of the shock also freezes and becomes "stabilized" for freestream Mach numbers close to one. Using the method of matched asymptotic expansions, Cook and Zeigler [9] showed that the local

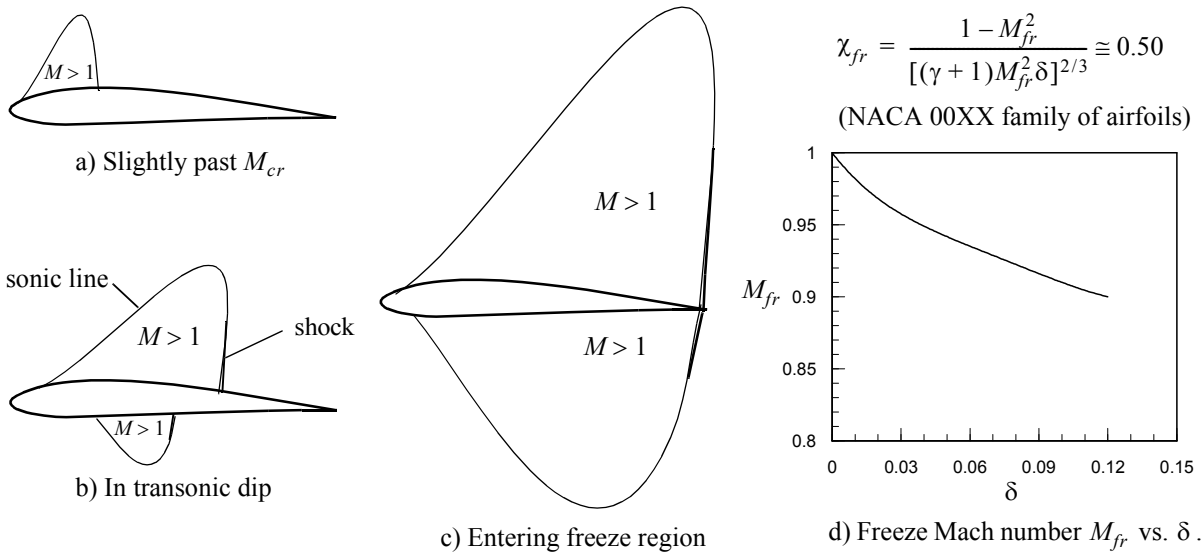

Figure 3: Mach number freeze and transonic stabilization of lift and moment coefficients.

Mach number differs from that at sonic flow ($M_\infty = 1$) only by terms of order χ^3, where χ is the transonic similarity parameter*

$$\chi = \frac{1 - M_\infty^2}{[(\gamma+1)M_\infty^2\delta]^{2/3}} \tag{2}$$

Here $\delta = t_{max}/c$ is the thickness-to-chord ratio, and γ is the ratio of specific heats.Thus, in the freeze region, the local Mach numbers on the upper and lower surfaces ahead of the shocks are given by

$$M_{u,l}(x/c, M_\infty) = M_{u,l}(x/c, 1) + O(\chi^3) \tag{3}$$

where x/c is the nondimensional chordwise location on the airfoil and the subscripts *u,l* denote the upper and lower surface, respectively. Since $\chi = 0$ at $M_\infty = 1$, Eq. (1) follows.

The airfoil pressure coefficient can be expressed in terms of the local and freestream Mach numbers, and making use of Eq. (3), we conclude that the stabilization of C_p, C_L and C_M ahead of the shocks are of the same form:

$$\begin{aligned} C_p(x/c, M_\infty) &= C_p(x/c, 1) + O(\chi^3) \\ C_L(M_\infty) &= C_L(1) + O(\chi^3) \\ C_M(M_\infty) &= C_M(1) + O(\chi^3) \end{aligned} \tag{4}$$

for fixed angle of attack and $M_{fr} \le M_\infty \approx 1 + \varepsilon$. Here M_{fr} is the corresponding freeze Mach number at which both the upper and lower shocks have reached the trailing edge; see Fig. 3.

Because the freeze only occurs ahead of the shocks on the upper and lower surfaces, a complete stabilization of the lift and moment coefficients does not occur until the shocks have reached the trailing edge. The scaling with respect to airfoil thickness follows from Eq. (2), keeping χ fixed. For example, as the thickness δ is reduced from 12% (NACA 0012) to 6% (NACA 0006), the freeze Mach number increases from 0.90 to 0.935. For the 3% thick NACA 0003 airfoil, the transonic similarity rule predicts a freeze onset at about Mach 0.958, Fig. 3d).

* In [8] an older form *K* of the similarity parameter was used, which has $(\gamma+1)M_\infty^2$ set equal to 1.

In [10] we made the following argument for the stabilization of lift and moment coefficients in unsteady flow. Consider a 2D airfoil section executing simple harmonic motion in pitch:

$$\alpha(t) = \alpha_0 e^{i\omega t} \tag{5}$$

For small amplitudes, the corresponding unsteady pressure coefficient can be written as the sum of the mean (average) coefficient and the unsteady oscillation about the mean:

$$C_p(x/c, M_\infty, t) = \overline{C}_p(x/c, M_\infty) + \Delta C_p(x/c, M_\infty, k)e^{i\omega t} \tag{6}$$

where the amplitude ΔC_p is considered complex to take care of any phase differences. In the freeze region, near Mach 1, the mean flow would become stabilized and $\overline{C}_p$ would freeze. For low reduced frequencies k, one would also expect the unsteady part to become stabilized as well, since in the quasisteady limit $k \to 0^+$ the motion can be considered a sequence of almost steady equilibrium states, with corresponding quasi-steady flows. Using this argument, one would expect that the unsteady C_p and thus also the unsteady C_L and C_M should freeze in roughly the same Mach number region as in steady flow.

Figure 4 shows results of unsteady Euler calculations for pure pitching oscillations about mid-chord for the NACA 0012 and NACA 0006 airfoils, as a function of reduced frequency and Mach number. The Mach number freeze phenomenon is clearly evident and leads to the expected stabilization of the unsteady lift amplitudes for $M_{fr} \le M_\infty \le 1 + \varepsilon$, where ε depends on the airfoil thickness and is of the order $\varepsilon = O(1 - M_{fr})$. The stabilization of the moment amplitude and phase is quite strong, and the onset of the freeze region is in good agreement with theoretical predictions. Also note that the aerodynamic phase becomes positive over a narrow range of transonic Mach numbers immediately before the freeze, indicating a SDOF torsional instability. The lift coefficient (not shown) also freezes [10]. It should be obvious that the strongly nonuniform behaviors of the lift and moment coefficients close to the Mach number freeze pose a challenge to the experimentalist as well as to anyone trying to validate CFD codes.

The influence of the Mach freeze on flutter was also considered in [10], using a 2D typical section model. In the Mach number freeze region, C_L and C_M differ from the corresponding values at sonic conditions by terms of order χ^3. Thus, the nondimensional unsteady aerodynamic load vector freezes around the loads corresponding to $M_\infty = 1$, to order χ^3:

$$\frac{\overline{U}^2}{\pi\mu}\begin{Bmatrix} -C_L(\tau) \\ 2C_M(\tau) \end{Bmatrix} = \frac{a_0^2\theta}{\pi b^2\omega_\alpha^2\mu} M_\infty^2 \begin{Bmatrix} -C_L(\tau) \\ 2C_M(\tau) \end{Bmatrix}_{M_\infty = 1} + O(\chi^3) \tag{7}$$

where a_0 is the speed of sound at SLSD conditions, $\theta = T/T_0$ is the absolute temperature ratio, $\tau = \omega_\alpha t$, $\dot{\alpha} = d\alpha/d\tau$, $\overline{U} = U_\infty/b\omega_\alpha$, and the standard Theodorsen notation has been used. For Mach numbers close to one, from M_{fr} to slightly beyond 1, the flutter boundary should be only a weak function of the free-stream Mach number. To keep the scaling factor in Eq. (7) frozen, we need

$$\frac{\theta}{\mu} M_\infty^2 = const. = \left.\frac{\theta}{\mu}\right|_{M_\infty = 1} \tag{8}$$

If the temperature is kept constant, this means that the critical mass ratio at flutter in the freeze region should scale as M_∞^2; that is, $M_\infty/\sqrt{\mu} = const.$ The dynamic pressure at flutter would then become frozen as well. However, the anomalous mass ratio scaling in the transonic region must also be considered in this context [11].

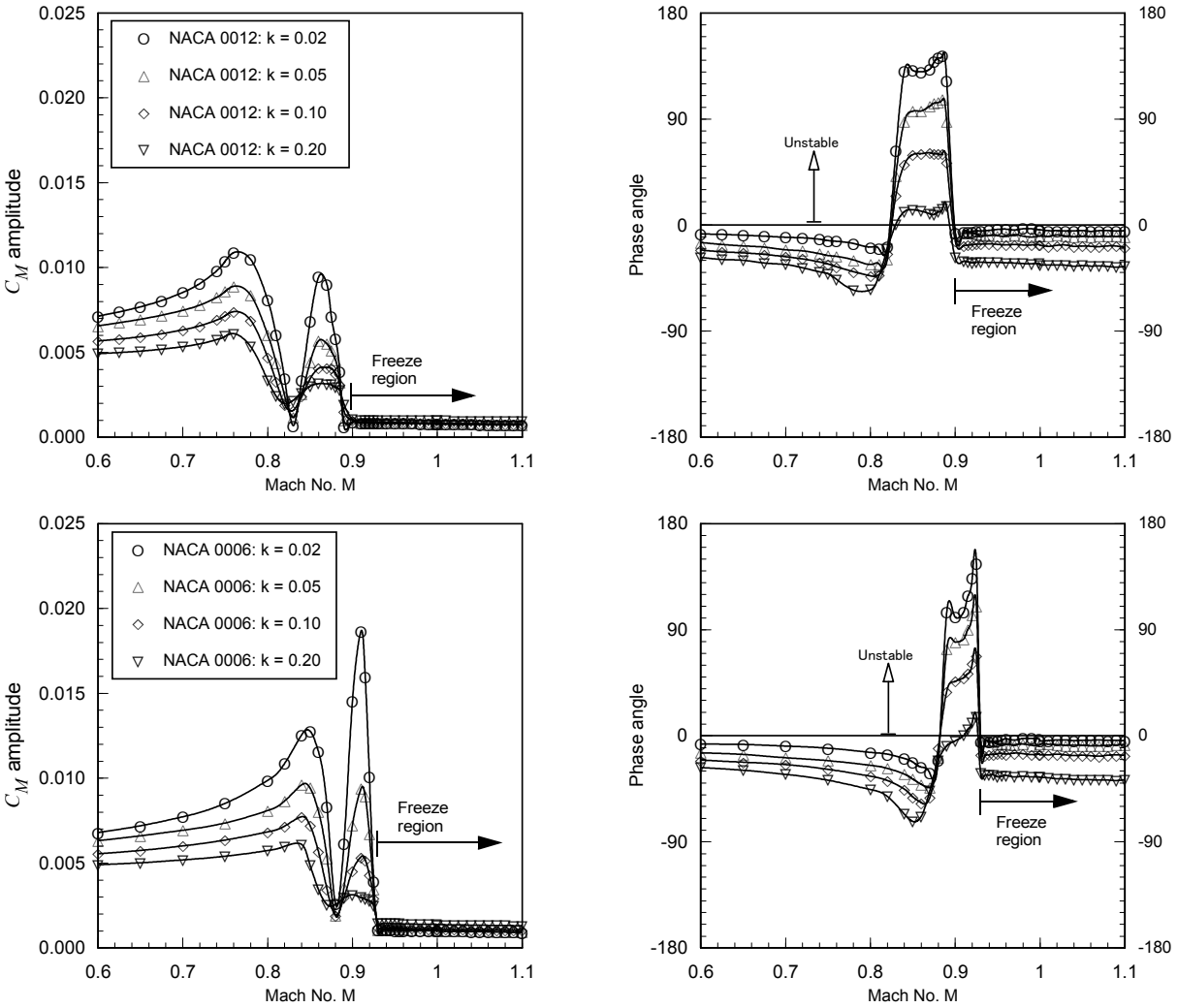

Figure 4: Unsteady moment amplitude and phase during pitching oscillations about midchord of NACA 0012 and NACA 0006 airfoils as a function of Mach number and reduced frequency $k = \omega b / U_\infty$ (Euler calculations; $\alpha_m = 0$; $\alpha_0 = 0.2°$). Note insensitivity of moment amplitudes to both Mach number and reduced frequency at high transonic Mach numbers (freeze region). From [10].

3 COMPUTATIONAL APPROACH

3.1 Direct FEM time-marching calculations

The computational model is based on a nonlinear finite element formulation of the fluid-structure system, implemented using a Galerkin finite element discretization of the Euler equations in the fluid domain and Mindlin-Reissner finite elements in the structural domain. The approach is a generalization of the Direct Eulerian-Lagrangian computational scheme, in which the calculations are done at the finite element level in both the fluid and structural domains [12]. The generalized forces associated with the in-plane and out-of-plane degrees-of-freedom are calculated in a local element-fixed Lagrangian coordinate system that fully accounts for large rigid body translations and rotations, thus removing the amplitude restriction inherent in the von Kármán plate theory.

The wing structure consists of a flat aluminum plate of the wing planform, covered with hard plastic foam to form the desired airfoil shape. This type of model construction was used in several early studies of transonic flutter at NASA Langley, such as the study of the effect of wing thickness on the transonic flutter boundary, by Doggett et al. [13]. It was also used more recently in the MAVRIC flutter model tested by Edwards et al. [14].

A multistage Runge-Kutta scheme is used to integrate the space-discretized system of nonlinear equations forward in time. Time accuracy is maintained by time-marching the fluid and structural finite element equations simultaneously, within the same 5-stage Runge-Kutta execution loop. Finite rotation relations are used to update the nodal displacement vectors at each stage, and the aerodynamic force vectors are calculated as follower forces, resulting in a more accurate prediction of the aeroelastic response. The exact nonlinear boundary condition at the wing surface is satisfied using the actual deformation of the wing, as defined by the finite element shape functions and the local element coordinates. For further details, see Ref. 15.

3.2 Flutter mode identification

To identify the aeroelastic modes involved in the LCOs, we project the time-accurate FE vector of generalized displacements on the linear eigenspace of natural modes. With this decomposition, we can calculate both the modal amplitudes as well as the kinetic energy contributed by each natural mode. This allows us to classify coupled aeroelastic modes where three or more modes contribute, which would not be possible based on the observed flutter frequencies alone. It has also been valuable in understanding "bursting" and "pseudorandom" flutter, where no single coherent flutter frequency emerges and the "modal content" of the nonlinear flutter mode is a function of time and often varies significantly over each flutter cycle.

3.3 Aerodynamic work calculations

In the nonlinear aeroelastic code used in the present study, time-accurate calculations of the net aerodynamic work ΔW_A per flutter cycle are carried out as a function of span location, at a total of 22 stations. The aerodynamic work data include the chordwise distribution of the aerodynamic work done by the fluid on the wing, per unit time and unit area. From this data it is possible to identify which wing sections extract energy and which sections dissipate energy. On a 3D wing, however, the aerodynamic work does not vanish at all span locations during an LCO flutter period; instead a balance is established between the positive and negative work such that the overall net aerodynamic work done on the wing is zero. Because this balance is sensitive to the local flow states in the stable and unstable regions, it is not surprising that the LCO amplitudes can be greatly affected by the presence of wing-mounted missiles and other stores, as experienced on the F-16 aircraft, for example.

In the strongly nonlinear transonic region, the LCOs usually arise from a delicate balance between the positive aerodynamic work done on the inner 60-70% of span and the negative work done on the outboard 30-40% of span (tip region). The boundary between the stable and unstable regions defines the *neutral section*, where the net work by the aerodynamic forces is zero over an LCO cycle.

By calculating the net aerodynamic work done when the wing is vibration in a pure natural mode, one can identify natural mode instabilities. If the work done is positive, the natural mode is unstable; if negative, it is stable. The aerodynamic work depends not only on the mode (1B, 2B, 1T, etc.), but also on the Mach number and the reduced frequency. If one considers a Mach number sweep at constant temperature, then the reduced frequency will vary inversely with the Mach number.

4 COMPUTATIONAL RESULTS - NESTED LIMIT CYCLES

4.1 Swept transport wing (G-wing)

The G-wing [5] (Fig. 5) is closely similar in planform to the wind tunnel model studied in Ref. 4, except that the two small trailing-edge kinks have been ignored. The airfoil section is the 10% thick ONERA “D” airfoil rather than the supercritical airfoil of the Göttingen wing [4].

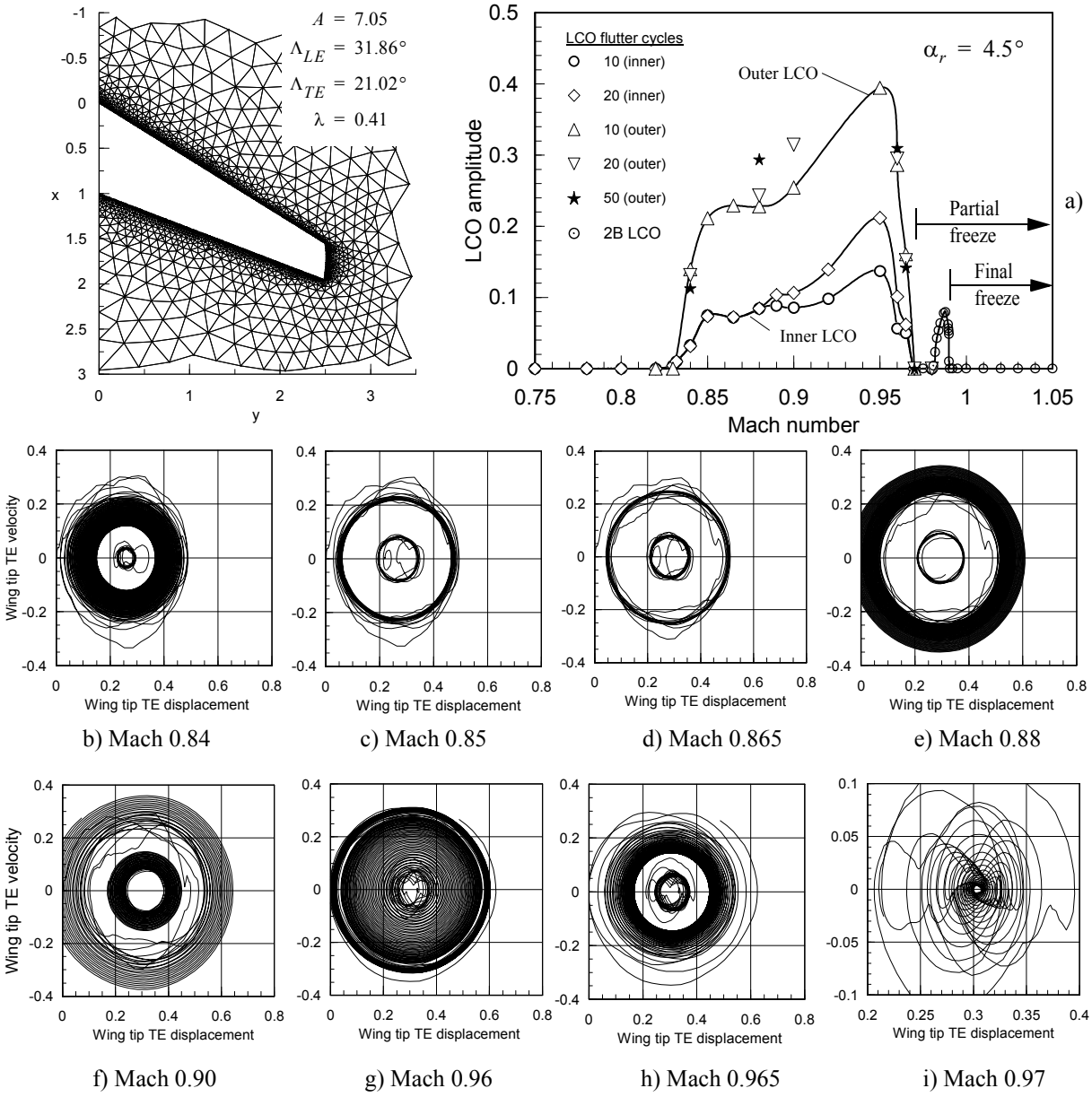

Figure 5: Multiple limit cycle flutter branches in transonic region at a density altitude of 10,000 m (32,800 ft): a) LCO amplitudes vs. Mach number; b)-i) LCO phase diagrams at 8 different Mach numbers in the LCO region. LCOs are weakly unstable in the Mach number range 0.88-0.95, but can be stabilized by increasing the air density (lower density altitude). (G-wing, Euler-based CFD and nonlinear structural FEM).

For swept wings of high aspect ratio, the structural washout mechanism has a strong influence on the wing streamwise pitching motion, and the effect on flutter can be profound and in some cases counterintuitive. In the case of the G-wing, a complex LCO-type flutter behavior was predicted by our calculations, involving two coexisting or nested limit cycles over a range of transonic Mach numbers between roughly 0.84 and 0.96 (Fig. 5). At Mach 0.97, both the inner and outer limit cycles "evaporate" and the wing amplitudes decay to zero, Fig. 5i). Around Mach 0.99, a second bending (2B) LCO reappears over a narrow Mach number region; see Figs. 5a) and 6.

The sudden quenching of the primary nested LCOs at Mach 0.97 is believed to be caused by the Mach number freeze phenomenon and the resulting transonic stabilization [10]. No plausible alternate physics-based explanations for the abrupt reversal of the LCO flutter amplitudes have

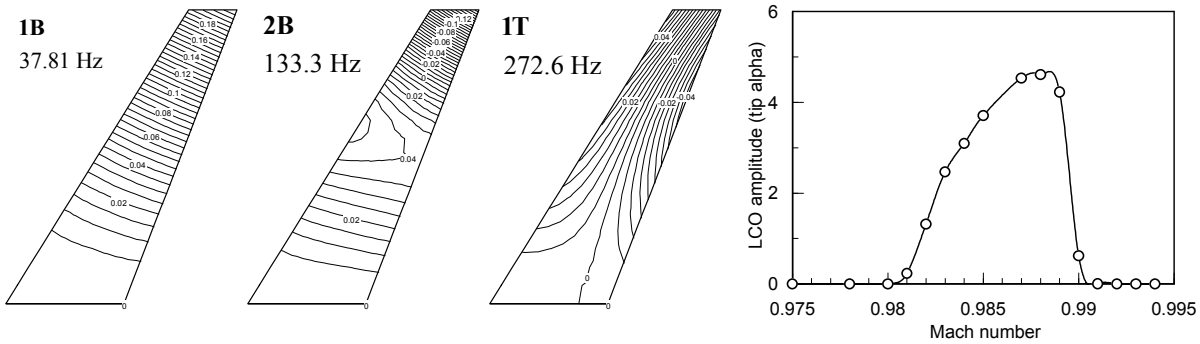

Figure 6: LCO pitch amplitude (°) at wing tip vs. Mach number for G-Wing LCO in the second bending (2B) mode. Contour plots of the first 3 modes are shown to the left in the figure.

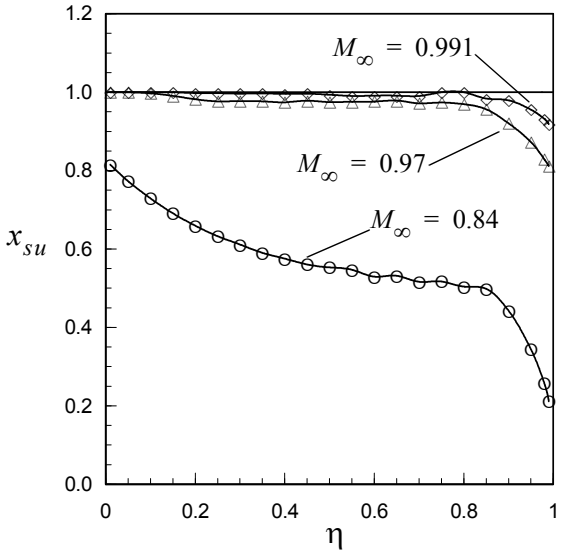

Figure 7: Chordwise location x_{sh} of the upper surface shock vs. span on the G-wing at three critical Mach numbers.

been found. The transonic stabilization of a swept high-aspect-ratio wing such as the G-wing is a three-dimensional mechanism. When the shocks on the inboard unstable section of the wing approach the trailing edge and the Mach number freeze sets in, the ability of the wing to extract energy from the airstream is severely reduced and eventually completely eliminated. This upsets the work balance between the inboard (unstable) and outboard (stable) region, resulting in a rapid and abrupt quenching of the LCOs. These "primary" LCOs are predominantly 1B branch instabilities (coupled 1B-1T). However, in the case of the second bending mode LCO, the situation is reversed: the tip region extracts energy and the inboard region dissipates energy. Therefore, the 2B LCO instability is not quenched until the shocks in the tip region get close to the trailing edge, which happens around Mach 0.991, Fig. 7.

4.2 ONERA M6 wing

Recent unsteady calculations for the aeroelastic model for the ONERA M6 wing studied previously in [12] have revealed similar reversals in the amplitudes and phases of the generalized aerodynamic forces associated with the natural modes of the wing. The first three modes are shown in Fig. 8. Aerodynamic work ΔW_A calculations indicate that ESDOF flutter instabilities are possible in the 1B, 1T, and 2B modes, for sufficiently low reduced frequencies; see Fig. 9. Surprisingly, the 5th and 7th modes also revealed instabilities just below Mach 1 (not shown). Also note that the instability regions differ for the individual modes and in the case of the 2B mode extends into the freeze region for very low reduced frequencies.

Figure 10 shows representative plots of the calculated aeroelastic response of the wing at Mach 0.85 at an air density of $\rho = 0.01\ kg/m^3$, verifying that the 1B mode is indeed weakly unsta-

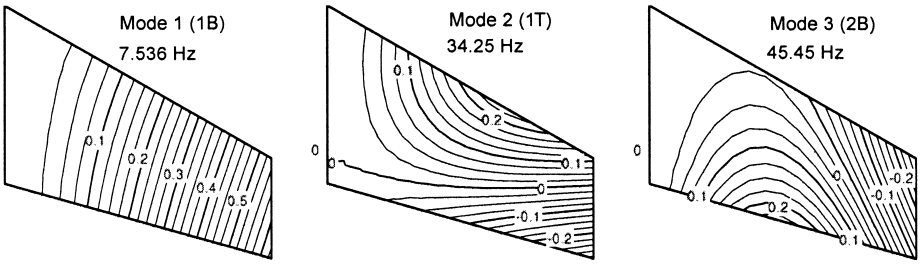

Figure 8: Contour plots of first three modes of the ONERA M6 wing.

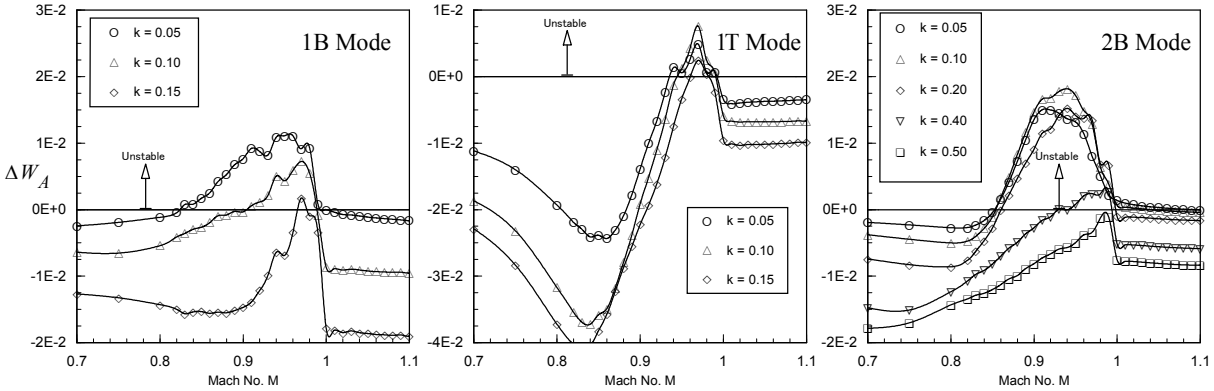

Figure 9: Aerodynamic work ΔW_A per cycle of the ONERA M6 wing oscillating in a pure natural mode (6th cycle; mean angle of attack 3 deg). For this wing, $M_{fr} \cong 1$ for all modes shown.

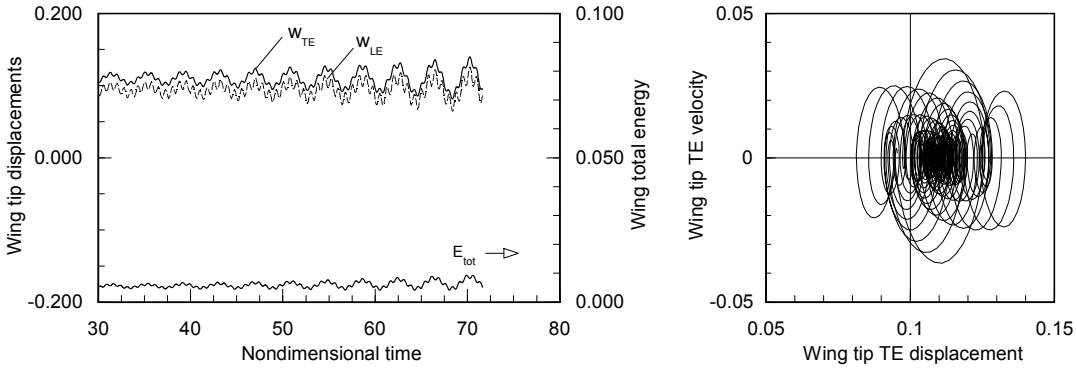

Figure 10: Transonic flutter of ONERA M6 wing at $M_\infty = 0.95$ and $\alpha_\infty = 3°$, showing emergence of 1B-2B multimode flutter ($\rho = 0.50\ kg/m^3$).

ble, as indicated in Fig. 9. The corresponding dynamic pressure is only 418.3 Pa (8.74 psf), and corresponds to a density altitude of more than 100,000 ft. In these calculations, the full FE structural model was used. This and other examples show that, at Mach numbers where modal instabilities are possible, the flutter boundary extends down to very low densities, corresponding to altitudes well into the stratosphere.

As the density or dynamic pressure is increased, the flutter mode gradually changes into a coupled bending-torsion mode wherein 1B still dominates, and the flutter instability becomes stronger. At Mach 0.95, the 1B, 2B, and 1T modes are all unstable at low reduced frequencies. Nested limit cycles in the 1B, 2B, and 1T modes would therefore be possible at and around Mach 0.95, under the right conditions. In a wind tunnel flutter test, one would expect to see weakly unstable LCOs at low dynamic pressures, which in the presence of structural damping might become weakly damped LCOs. At higher dynamic pressures/densities, strong bending-torsion flutter

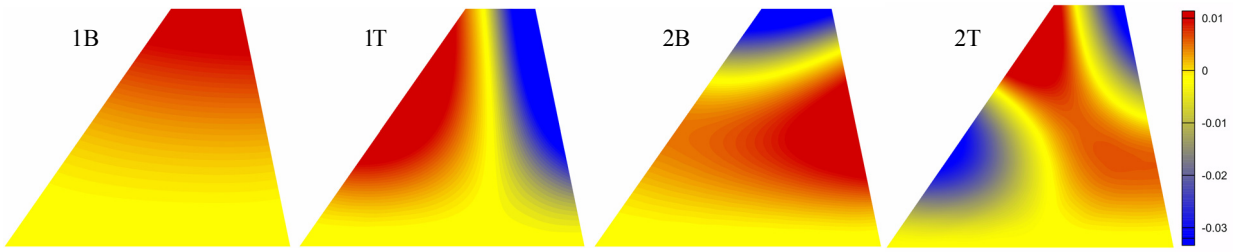

Figure 11: First four modes of the FX-wing model ($c_r = 40$in).

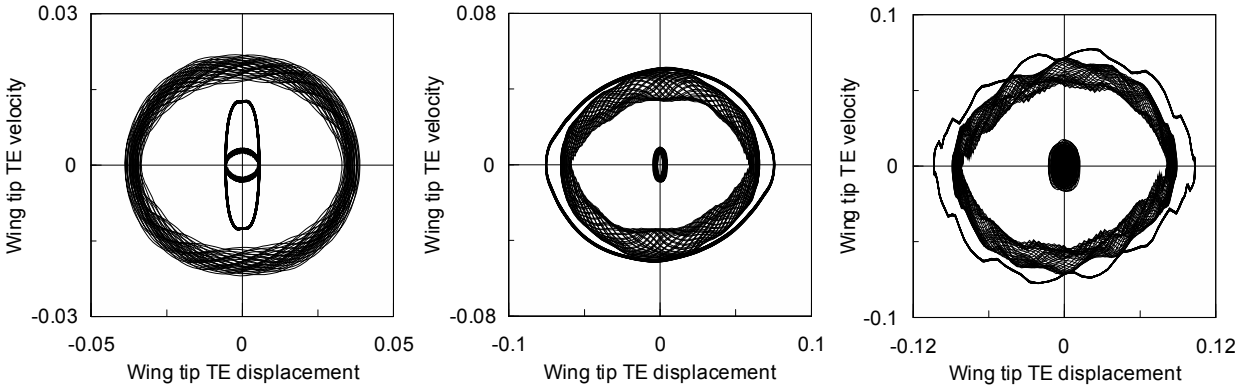

a) $\rho = 0.02\ kg/m^3$; $q = 23.7$ psf b) $\rho = 0.08\ kg/m^3$; $q = 94.8$ psf c) $\rho = 0.10\ kg/m^3$; $q = 118.5$ psf

Figure 12: Phase plots of 3 different nested limit cycles occurring at Mach 0.99 (FX-wing).

would be expected. This situation is qualitatively similar to that observed in the wind tunnel tests of several different swept wings reported in [14,16-20].

4.3 Advanced fighter wing (FX-wing)

The FX wing planform is representative of 5th and future 6th generation fighters, with a LE sweep of 35 deg, a TE forward sweep of 11.7 deg, and a taper ratio of 0.245. The aspect ratio is 2.67. The first four mode shapes are shown in Fig. 11 and display the plate mode features typical of low aspect ratio fighter wings.

Calculations show that the FX wing has multiple or nested limit cycles at Mach numbers near one. In most cases the "inner" low-amplitude LCO is essentially a natural mode instability in the second bending (2B) mode of the wing, whereas the "outer" high-amplitude LCO is typically a coupled mode dominated by first bending (1B). Aerodynamic work ΔW_A calculations indicate that ESDOF flutter instabilities are possible in the 2B mode, but not in the 1B or 1T modes. At Mach numbers where nested LCOs are possible, the flutter response becomes sensitive to initial conditions. If the initial disturbances are sufficiently small, the flutter mode is attracted to the inner low-amplitude LCO. At small to moderate air densities (or dynamic pressures), the outer LCO can only be reached through a sufficiently large initial disturbance, or from the inner LCO if a short burst of negative damping is introduced via a suitable control parameter. At high dynamic pressures, the long-term aeroelastic response typically converges to the outer LCO. However, if the initial condition is in the 2B mode, the flutter response can be made to converge to the inner LCO even at moderately high dynamic pressures.

Figure 12 shows the presence of 3 nested LCO at Mach 0.99. The outer LCOs are dominated by the 1B mode, coupled nonlinearly to the 1T and 2B modes. In a) the inner LCO is a small 1B-2B mode and the intermediate LCO is a 2B mode. Only the 2B mode is unstable as a natural

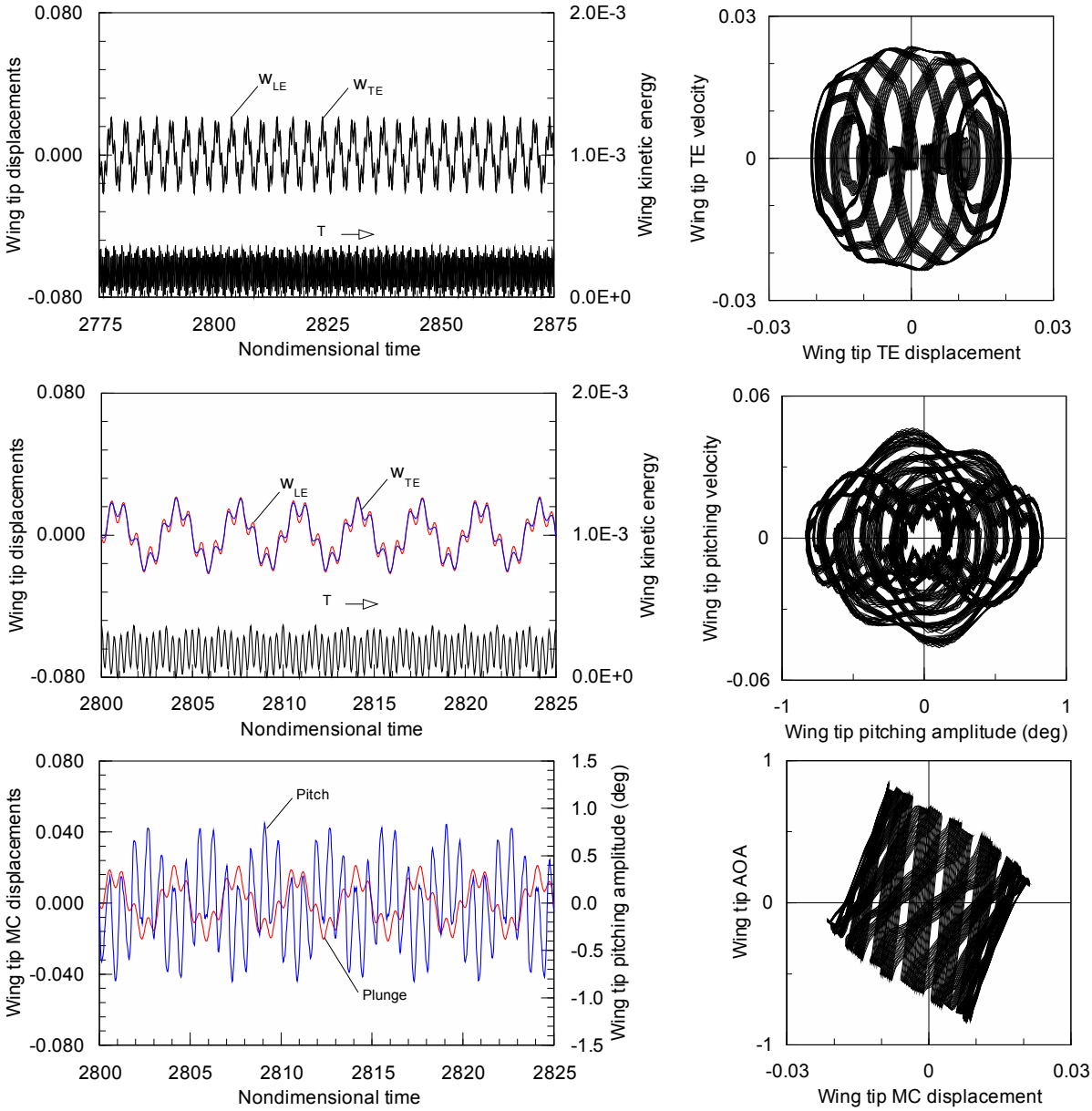

Figure 13: Nonclassical LCO arising from nonlinear interactions between the 1B and 2B modes of the FX-wing at Mach 0.99 and $\rho = 0.05\ kg/m^3$; 59.3 psf. Motion is not periodic, but may be almost periodic in the sense of the theory of H. Bohr [22]. Initial conditions in 1B mode.

mode (Fig. 12), thus the other two nested LCOs are coupled modes where the 2B mode is the driver at low dynamic pressures. In b) and c), the inner LCO is a weakly unstable 2B mode and the intermediate LCO is a complex and highly nonlinear 1B-2B-1T coupled mode.

Figures 13-15 shows detailed plots of the flutter modes involved in the 3 nested LCOs at Mach 0.99 and an air density of $\rho = 0.05\ kg/m^3$, corresponding to a dynamic pressure of $q = 59.3$ psf. The time traces of the bending displacements at the wing tip leading and trailing edges reveal a modulated LCO, resulting from nonlinear interactions between two or more modes. These are nonclassical flutter modes where the structural modes participating do not become synchronized and a distinct flutter frequency does not emerge.

Figure 13 reveals a complex banded structure in the phase plots, most likely arising from motion on a torus in phase space. The initial conditions are in the first bending (1B) mode and the aeroelastic calculations cover about 116 seconds of real time (2,875 in nondimensional time).

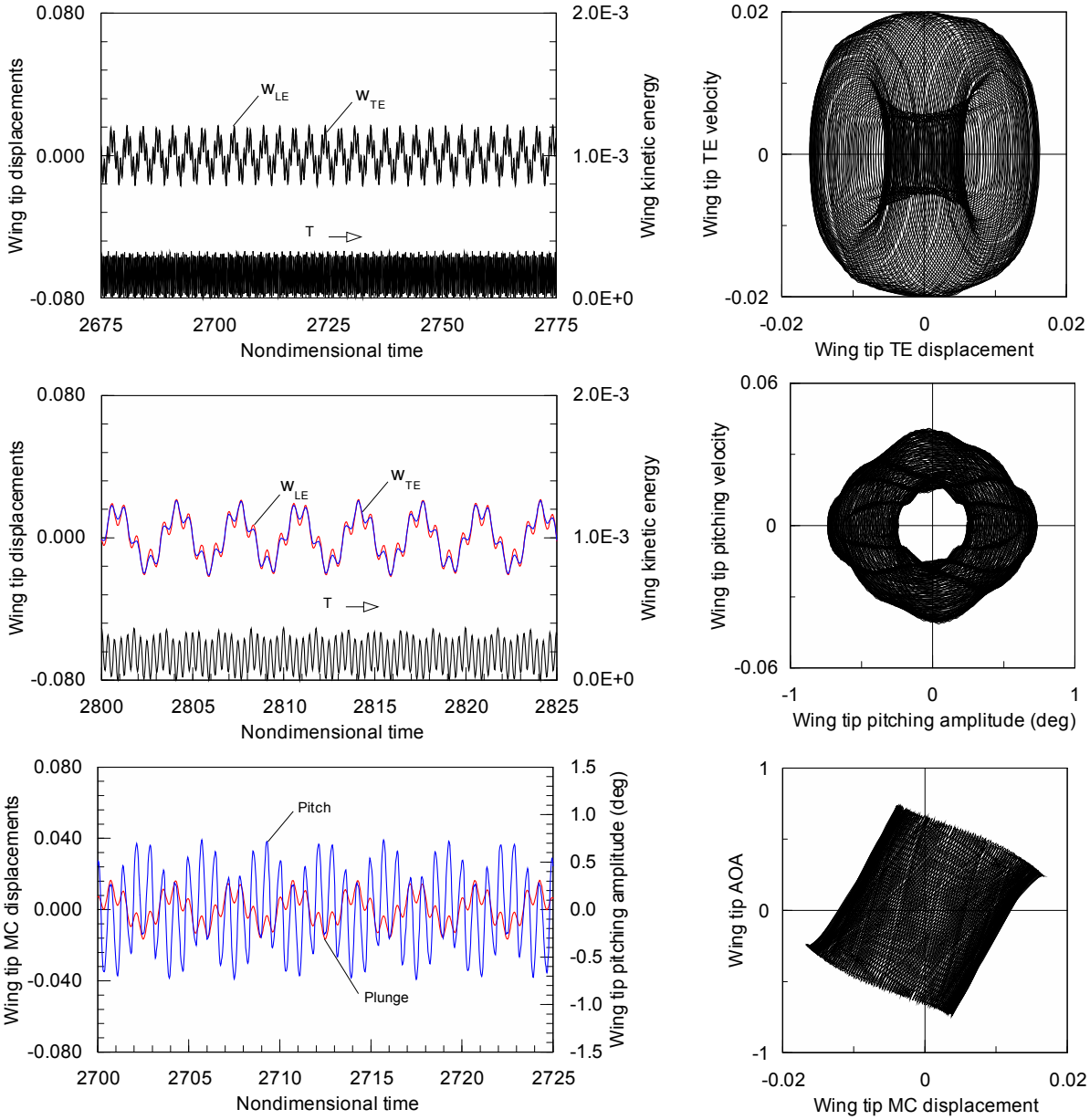

Figure 14: Same case as in Fig. 13, except for initial conditions. Calculations were started from a run at $\rho = 0.02\ kg/m^3$ (with 1B initial conditions) that had completed a run of about 51.8 seconds duration.

Figure 14 shows the same case, but started from a converged multimode LCO at a lower density ($\rho = 0.02\ kg/m^3$) that had completed roughly 51.8 seconds (1,284 in nondimensional time). The run continues for an additional 112 seconds, of which only the last 4 seconds are shown in the figure. The wing tip displacement time traces look similar to those in Fig. 13, but the phase plots clearly show a different dynamical mode. The LCO is a coupled 1B-2B mode. Again, the flutter mode appears to represent motion on a torus.

Figure 15 shows the case with the initial conditions in the second bending mode. The initial response (not shown) is essentially a clean 2B LCO, which through weak nonlinear interactions with the 1B mode (and to a lesser degree the 1T mode), converges to the multimode LCO shown in the plots. The mode differs from the previous two in that the plot of the kinetic energy T is very "clean", with a definite amplitude and no temporal spikes.

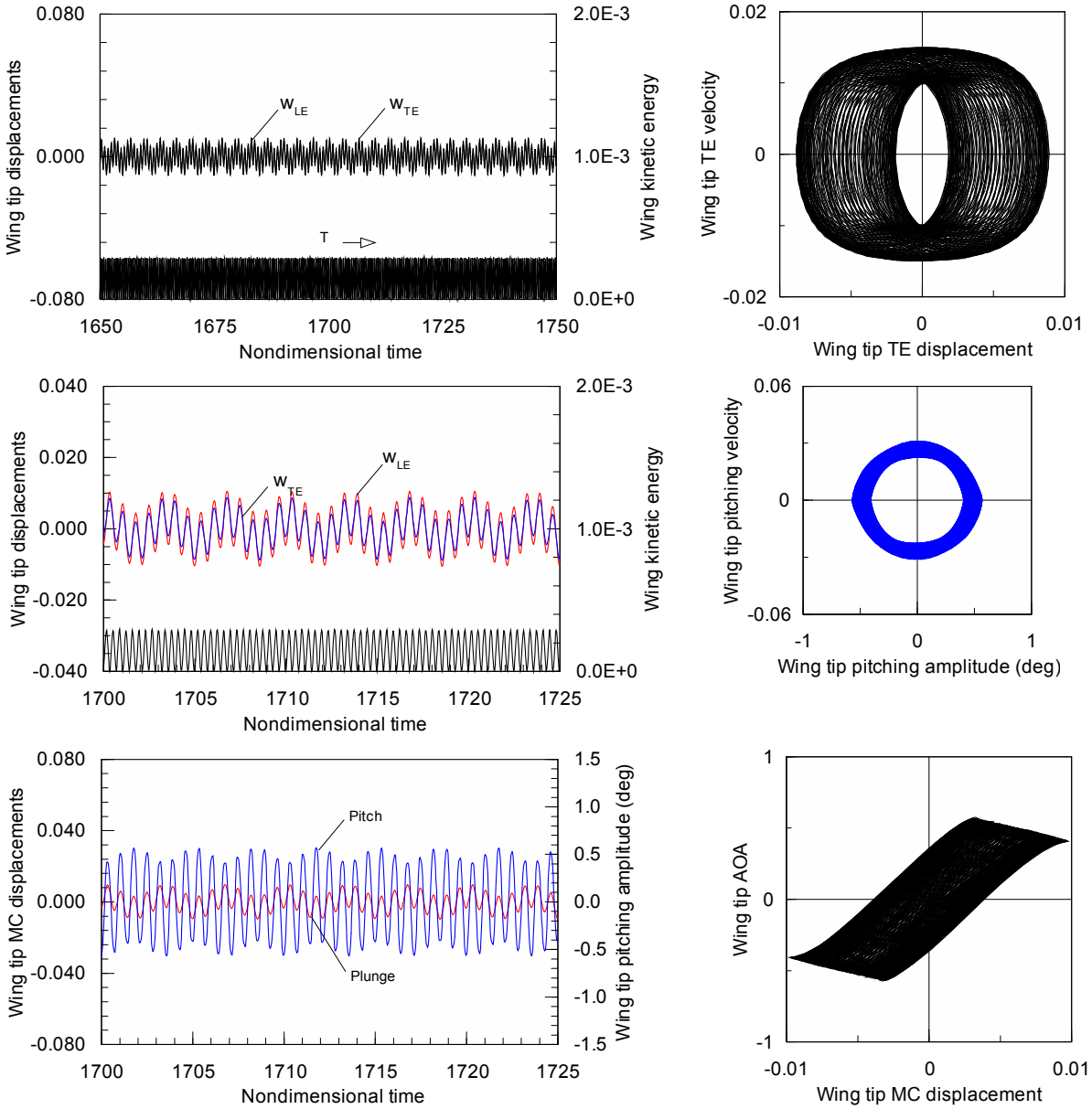

Figure 15: Second bending LCO with weak nonlinear interactions with 1B and 2T modes (FX-wing at Mach 0.99 and $\rho = 0.05\ kg/m^3$; 59.3 psf). Initial conditions in 2B mode. Simulation covers about 70.6 seconds.

4.4 Natural mode instabilities of flexible wings

Several instances of what appears to be "natural mode LCOs" have been observed in wind tunnel and flight tests [14,16-20], and several possible explanations of the physical mechanisms behind the instabilities have been put forth. In the B-1 case, the initial explanation [16] in terms of shock-induced separation was later changed to a (LE) vortex-induced instability [17]. In the wind tunnel tests of the elastic supercritical wing reported in [18], the observed bending mode LCO at high transonic Mach numbers was attributed to intermittent separation and reattachment of the flow in the trailing edge region behind the shock. During transonic wind tunnel tests of the HSCT wing [19], a region of "increased response" in the first bending mode was noted, and a narrow "chimney" of LCO-type flutter was observed around Mach 1. Similar narrow regions of natural mode instabilities in 1B, 1T, and 2B were also observed during wind tunnel testing of the MAVRIC wing [14].

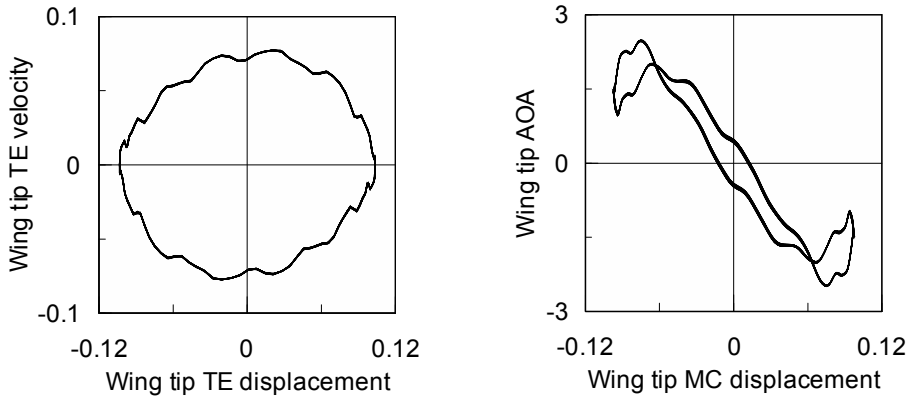

a) Converged large-amplitude 1B LCO from 1B i.c. (about 20 seconds elapsed time).

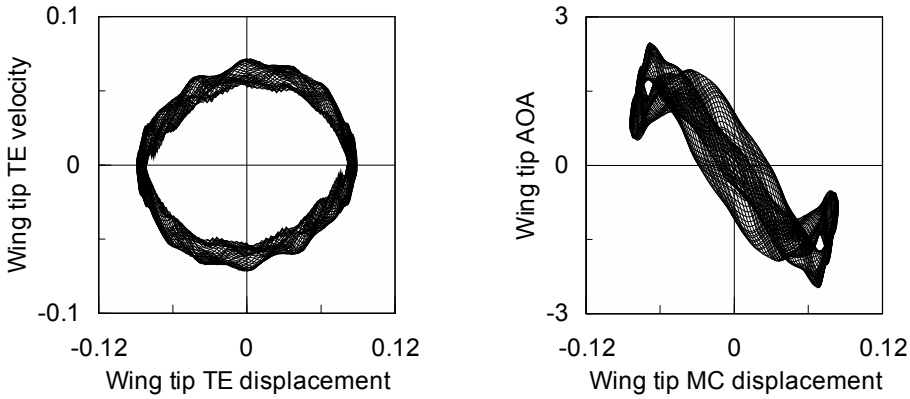

b) Converged large-amplitude complex mode from 2B i.c. (about 68 seconds of elapsed time).

Figure 16: Illustrating sensitivity to initial conditions at transonic conditions (FX-35 NACA 64A006 TDT model; $M_\infty = 0.99$ $\rho = 0.10\ kg/m^3$; $q = 118.52$ psf).

These experimental results share certain important traits:

1. The LCO-type instabilities require transonic (mixed) flows and are not observed in purely subsonic or supersonic flows.
2. The LCO amplitudes show a marked sensitivity to angle of attack, especially in the case of highly swept wings representative of supersonic planforms.
3. The instability region for a given natural mode is narrow, and the mode usually becomes stabilized by a small increase in Mach number.

Strictly speaking, no "pure" SDOF flutter instabilities are possible in 3D, because aeroelastic deformations will alter the flutter mode slightly, and the flutter will therefore not be SDOF flutter as in the 2D typical section case. However, in the limit as the air density goes to zero, the mode approaches the corresponding natural mode asymptotically, and if unstable, will essentially correspond to a SDOF instability in a single natural mode of the wing. It seems appropriate to call this type of modal instability *Essentially Single-Degree-of-Freedom* (ESDOF) flutter [21].

As in the case of the ARW-2 wing, it is difficult to explain the narrowness of the LCO chimneys without invoking the Mach number freeze and the associated stabilization of the unsteady aerodynamic forces acting on the wing. In [14] it is concluded that the LCO behavior "appears to be due to a very fine balance of forces on the wing, occurring at conditions of intermittent flow separation over wing regions of dominant modal motions (e.g., the wing-tip region here for the first bending and torsion modes)." It is not clear if the authors are referring to the aerodynamic forces only, or to the sum of aerodynamic, structural, and inertial forces (which of course must

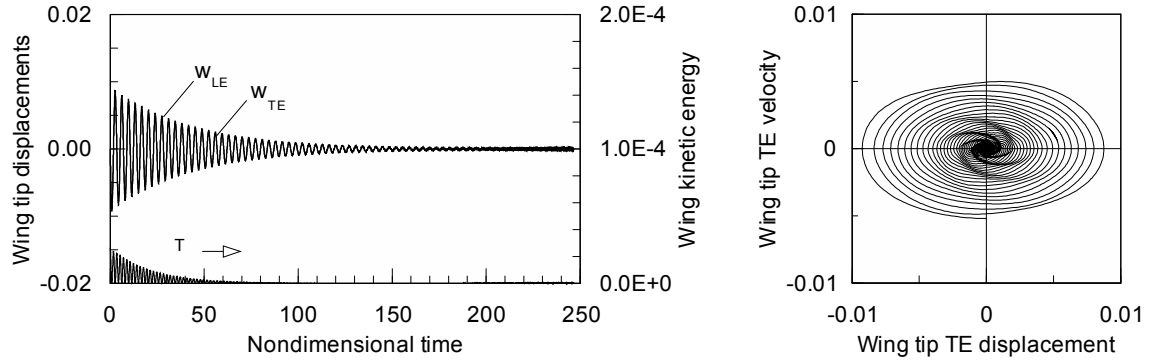

a) First 10 seconds after initial conditions in 1B mode

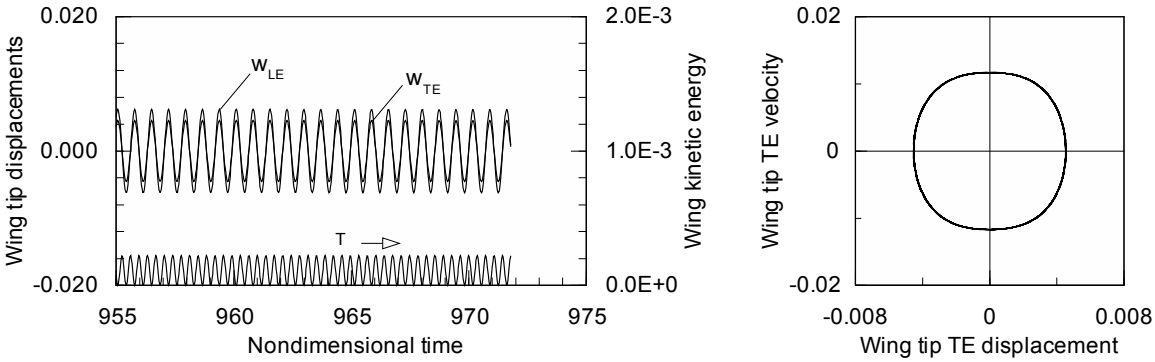

b) Final convergence to 2B LCO after almost 40 seconds.

Figure 17: Secular aeroelastic mode transition from 1B to 2B at Mach 0.92 and $\rho = 0.05\ kg/m^3$; $q = 51.18$ psf (FX-NACA 64A006 TDT wing model).

balance as required by the momentum conservation laws and d'Alembert's Principle). The aerodynamic forces by themselves are not in balance, but for a clean LCO with a fixed amplitude the net aerodynamic work done by these forces must balance over an LCO cycle; i.e., $\Delta W_A = 0$. For a "dirty" LCO, where the amplitude is only constant in a statistical average sense over a time interval T containing many LCO periods, and where the LCO frequency may not be clean either, one can invoke the Bohr theory of almost periodic (a.p.) functions [22] and take the average in the limit $T \to \infty$

$$\overline{W}_{A_\infty} = \lim_{T \to \infty} \frac{1}{T} \int_0^T W_A dt \tag{9}$$

If $\overline{W}_{A_\infty}$ approaches a fixed value, it seems reasonable to assume that the aeroelastic oscillations define an LCO in an average a.p. sense.

Calculations of ΔW_A for a swept transport wing similar to the MAVRIC (the G-Wing) show that the situation is more complex than assumed in [14]; see [21]. The inner and outer LCOs in the Mach number range 0.84-0.96 are in fact the result of a delicate balance of ΔW_A over the span of the wing, but ΔW_A does not vanish at all span locations. Instead, there is overall "integrated" spanwise balance over the wing during LCO-type flutter. This type of spanwise work balance is not possible in 2D, i.e., for a typical section wing model.

4.5 Flutter mode transitions

Figure 17 shows a "secular" (very slow) aeroelastic mode transition from the 1B mode to the 2B mode for the FX-NACA 64A006 wing model at Mach 0.92. At this Mach number, the 1B mode is stable, but the 2B mode is unstable. From linear aeroelasticity theory, one would expect the 2B mode to emerge immediately, independent of the presence of the 1B mode, but this does

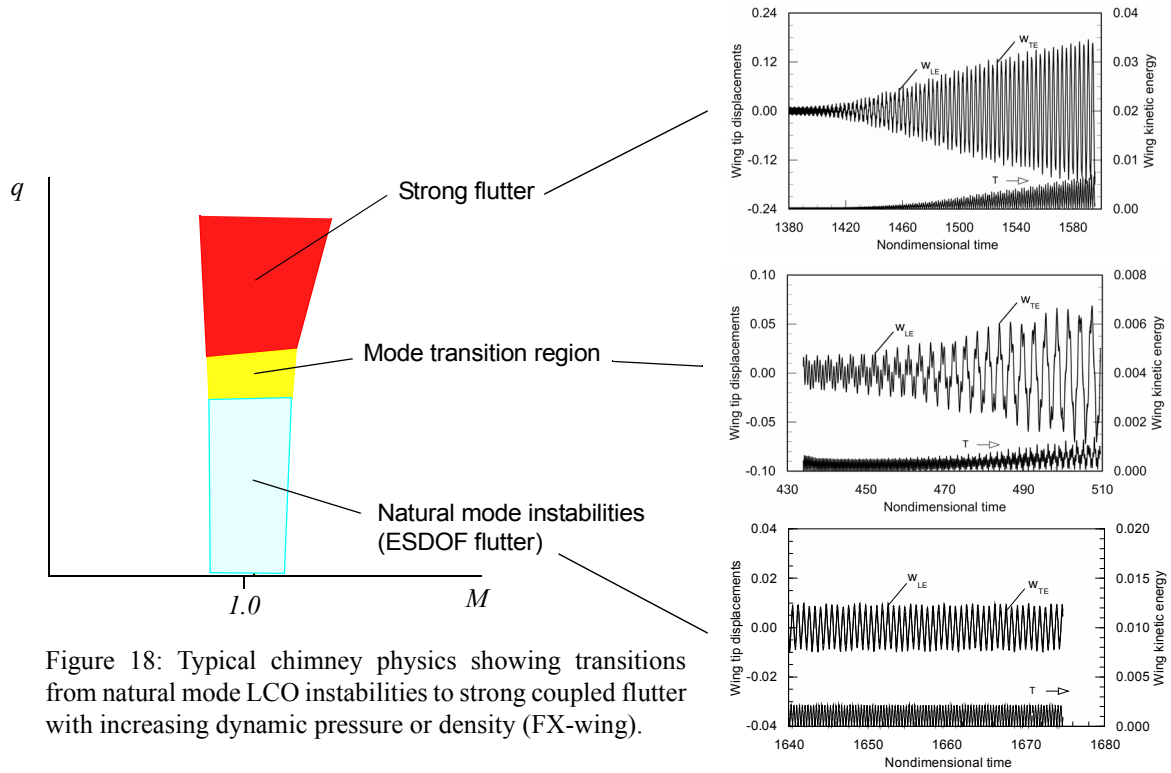

Figure 18: Typical chimney physics showing transitions from natural mode LCO instabilities to strong coupled flutter with increasing dynamic pressure or density (FX-wing).

not happen. Instead, the 2B instability appears quenched by the 1B mode, until the 1B amplitudes have decayed to near zero (after about 7-8 seconds). As can be seen from the figure, it takes almost 40 seconds to reach the final 2B LCO amplitude. In all figures in this paper, time is nondimensionalized with respect to the period of the first torsion (1T) mode. For the FX -wing, this translates to about 4 seconds for each nondimensional time interval of 100.

As expected from the transonic similarity laws, the 2B instability region depends on the airfoil thickness. For the FX-wing model with an NACA 64A003 airfoil, aerodynamic work calculations indicate that the unstable region starts around Mach 0.942 and ends around Mach 1.23. With the NACA 64A006 airfoil, the unstable region is between Mach 0.907 and 1.16. The change in the start of the 2B instability between the two airfoils is in good agreement with the predictions of the similarity laws; however, the supersonic ending Mach number for the NACA 64A003 airfoil is somewhat higher than expected from the similarity rules. This may be caused by a nonlinear reduced frequency effect.

Figure 18 shows typical flutter behavior of the FX-wing in the chimney around Mach 1. At low densities, the second bending (2B) mode dominates, with the first bending mode (1B) emerging as the density is increased. In the middle of the chimney, around Mach 1, rapid changes in the flutter mode are observed. With increasing density or dynamic pressure, a transition to a strong coupled 1B-2B flutter mode occurs inside the chimney; see Fig. 18. Because the coupling between the modes is essentially nonlinear, through aerodynamic and structural nonlinearities, the phase plots are not representative of "clean" limit cycles as observed in classical nonlinear dynamical systems. The structural modes participating are not synchronized and a distinct flutter frequency does not emerge. However, the modal decomposition procedure described in Sec. 3.2 can still be used to identify the modes participating and classify the flutter mechanism(s) involved.

4.6 Nonstationary "bursting" flutter

At some combinations of Mach numbers and dynamic pressures, a "bursting" or "pseudorandom" response occurs (Fig. 19). There may be several causes for nonstationary or "stochastic"

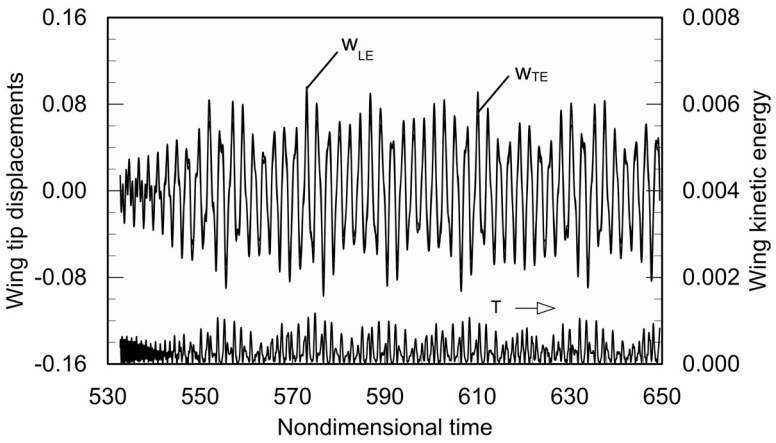

Figure 19: Bursting or pseudorandom flutter response at Mach 1.02 and high dynamic pressure (FX-wing; $\rho = 0.20$ kg/m^3; $q = 257.6$ psf; $\alpha_\infty = 0°$).

flutter. In the results obtained in this study, we believe that the main driver is a strongly nonlinear interaction between 2 or 3 modes of the wing, which is nonclassical in the sense that the aeroelastic response of the coupled modes never become synchronized, as in classical linear flutter. Bursting or pseudorandom flutter was observed during testing of a 2D supercritical wing at DLR [23], and during testing of the MAVRIC wing at NASA Langley [14].

4.7 Physical mechanisms behind nested LCOs

To date, explanations for the often complex LCO instabilities seen in wind tunnel tests at transonic Mach numbers have largely been based on visual observations alone (e.g., of shock-induced separations, etc.). However, necessary and sufficient conditions for these instabilities cannot be based entirely on visual observations, but must ultimately be based on energy/aerodynamic work considerations. That is, the proposed instability mechanism must be capable of extracting net energy from the airstream over a suitable time scale, such as one period of oscillation. Furthermore, the instability mechanism must depend on the flutter amplitudes so as to throttle the aerodynamic work and produce an LCO rather than exponentially growing flutter.

Within this framework, any hypothetical LCO mechanism can be tested computationally as well as experimentally, by determining whether it results in $\Delta W_A > 0$ (destabilizing) or $\Delta W_A < 0$ (stabilizing) upon its introduction. Of course, an experimental verification would be quite challenging because of the extensive instrumentation needed to obtain the required time-accurate unsteady pressures and wing surface displacements and velocities. The data obtained on the ARW-2 and the MAVRIC wings, although extensive by past aeroelastic testing standards, are not sufficient to make such calculations possible. In addition to time-accurate unsteady pressure data, one would need time-accurate displacement and velocity data on the wing surface collocated with the pressure measurements.

Based on the results of this study to date, we have identified three primary mechanisms:

1. Natural mode instabilities ahead of the Mach freeze.
2. Coupled or ESDOF aeroelastic modes with spanwise aerodynamic work balance and where a neutral section exists (only possible for 3D wings).
3. Nonlinear interactions between two or more modes where ΔW_A exists only in a stochastic sense; see Eq. (9).

5 CONCLUDING REMARKS

There are several computational as well as experimental implications of the observed multiple nested limit cycles. First, calculations to date indicate that the whenever two or more nested

LCOs are present, the lower LCO often becomes unstable (or semistable) in a certain Mach number range, essentially vanishing, or having such a narrow basin of attraction that it is for all practical purposes unobservable. Different codes using different CFD algorithms would most likely obtain different LCO stability behaviors, which could result in some codes marching past the weakly attracting lower LCO and converging to the outer LCO.

Second, extended flutter calculations show that the upper LCO may become unstable, even if the lower LCO is stable. In an experimental setting (wind tunnel or flight test), this could be dangerous, because a small change in Mach number or dynamic pressure could transform a benign LCO into hard flutter.

Third, the existence of multiple LCOs and the possible morphing between semistable and stable LCOs brings up important code verification and validation issues. The logical separation of the verification step (solving the equations right) and the validation step (solving the right equations) breaks down, and the two steps may become impossible to separate from a practical standpoint. The experimentalist is faced with similar difficulties in trying to understand the flutter test results and "validate" the experimental data. In aeroelastic systems exhibiting multiple LCOs sensitive to initial conditions and control parameters, this is a daunting problem that may require new experimental and computational techniques.

It seems reasonable in a paper that deals with multiple limit cycles to mention Hilbert's 16^{th} Problem, and attempt to learn from more than a century of research on this apparently simple problem. Although referred to as a two-dimensional problem in the mathematics literature, it is a single-degree-of-freedom problem from a dynamics standpoint, with an analytic right-hand-side. In state-variable form, the two equations have right-hand sides consisting of polynomials of degree n. Hilbert's 16^{th} problem is concerned with determining the upper bound on the number of limit cycles possible for a given polynomial degree n. This problem has not been solved yet, even for low values of n. According to a conjecture by Dulac [24], the number of limit cycles of a two-dimensional system with an *analytic* right-hand-side is finite, whatever its number may be. For a long time, it was believed that a quadratic system ($n = 2$) could at most have 3 limit cycles, but in 1980 [25] a counterexample with 4 limit cycles was constructed. If a SDOF system with analytical forces and algebraic nonlinearities cannot be understood from a theoretical standpoint, what hope is there for the general multi-degree-of-freedom nonlinear aeroelastic problem, where the unsteady aerodynamic forces are not analytic functions of the state of the system, except in simple quasisteady or truncated (finite state) aerodynamic models?

Acknowledgments

This research was supported by AFOSR Contract FA9550-13-C-0016 through a subcontract from Creative Aero Engineering Solutions, Long Beach, CA.

References

[1] Schewe, G., Knipfer, A., Mai, H., and Dietz, G., "Nonlinear Effects in Transonic Flutter" *Int. Forum on Structural Dynamics and Aeroelasticity 2001*, Madrid, Spain, June 2001.

[2] Schewe, Mai, H., and Dietz, G., "Nonlinear Effects in Transonic Flutter with Emphasis on Manifestations of Limit Cycle Oscillations" *Journal of Fluids and Structures,* Vol. 18, No. 1, 2003, pp. 3-22.

[3] Bendiksen, O.O., "Transonic Limit Cycle Flutter/LCO," AIAA Paper 2004-1694, April 2004.

[4] Dietz, G., Schewe, G., Kiessling, F., and Sinapius, M., "Limit-Cycle-Oscillation Experiments at a Transport Aircraft Wing Model," *Proc. International Forum on Structural Dynamics and Aeroelasticity 2003*, Amsterdam, The Netherlands, June 4-6, 2003.

[5] Bendiksen, O.O., "Transonic Limit Cycle Flutter of High-Aspect-Ratio Swept Wings,"

Journal of Aircraft, Vol. 45, No.5, September-October 2008, pp. 1522-1533.

[6] Bendiksen, O.O., "Multiple Limit Cycles in Transonic Flow and Some Computational and Experimental Implications," Paper AVT-152-024, *NATO AVT-152 Symposium on Limit Cycle Oscillation and Other Amplitude-Limited Self Excited Oscillations*, Loen Norway, May 5-8, 2008.

[7] Cole, J.D., "Modern Developments in Transonic Flow," *SIAM Journal of Applied Mathematics*, Vol. 29, No. 4, December 1975, pp. 763-787.

[8] Cole, J.D., "Review of Transonic Flow Theory," AIAA Paper 82-0104, 1982.

[9] Cook, L.P., and Zeigler, F.J., "The Stabilization Law for Transonic Flow," *SIAM Journal of Applied Mathematics*, Vol. 46, No. 1, February 1986, pp. 27-48.

[10] Bendiksen, O.O., "Transonic Stabilization Laws for Unsteady Aerodynamics and Flutter," AIAA Paper 2012-1718, *Proc. 53rd AIAA/ASME/ASCE/AHS/ASCE SDM Conf.*, Honolulu, HI, April 23-266, 2012.

[11] Bendiksen, O.O., "Review of Unsteady Transonic Aerodynamics: Theory and Applications," *Progress in Aerospace Sciences*, Vol. 47, Issue 2, February 2011, pp. 133-167.

[12] Bendiksen, O.O., "Modern Developments in Computational Aeroelasticity," *Journal of Aerospace Engineering, Proc. Inst. Mechanical Engineers*, Part G., Vol. 218, No. 3, June 2004, pp. 157-178.

[13] Doggett, R. V., Jr., Rainey, A. G., and Morgan, H. G., "An Experimental Investigation of Aerodynamic Effects of Airfoil Thickness on Transonic Flutter Characteristics," *NASA TM X-79*, 1959.

[14] Edwards, J.W., Schuster, D.M., Spain, C.V., Keller, D.F., and Moses, R.W., "MAVRIC Flutter Model Transonic Limit Cycle Oscillation Test," *Proceedings of the International Forum on Aeroelasticity and Structural Dynamics (IFASD 2001)*, Madrid, Spain, June 2001, pp. 581-595.

[15] Bendiksen. O.O., and Seber. G., "Fluid-Structure Interactions with both Structural and Fluid Nonlinearities," *Journal of Sound and Vibration*, Vol. 315, Issue 3, 19 August 2008, pp. 664-684.

[16] Stevenson, J.R., "Shock-Induced Self-Exited Airfoil Bending Oscillations," Rockwell International paper presented to the Aerospace Flutter and Dynamics Council, Las Vegas, NV, Oct. 19-20, 1978.

[17] Dobbs, S.K., Miller, G.D., and Stevenson, J.R., "Self-Induced Oscillation Wind Tunnel Test of a Variable Sweep Wing," AIAA Paper 85-0739-CP, 1985.

[18] Seidel, D.A, Eckstrom, C.V., and Sandford, M.C., "Transonic Region of High Dynamic Response Encountered on an Elastic Supercritical Wing," *Journal of Aircraft*, Vol. 26., No. 9, September 1989, pp. 870-875.

[19] Silva, W., et al., "Experimental Steady and Unsteady Aerodynamic and Flutter Results for HSCT Semispan Models," *AIAA Paper 2000-1697*, 2000.

[20] Machida, S., Kichuchi, T., Arizono, H., and Saitoh, K., "Transonic Flutter Characteristics of an Arrow Wing Mounted with Engine," AIAA Paper 2005-835, 2005.

[21] Bendiksen, O.O., "Transonic Single-Degree-of-Freedom Flutter and Natural Mode Instabilities," AIAA Paper 2013-1593, *Proc. 54th AIAA/ASME/ASCE/AHS/ASCE SDM Conf.*, Boston, MA, April 8-11, 2013.

[22] Bohr, H., *Almost Periodic Functions*, Chelsea Publishing Company, New York, NY, 1947.

[23] Knipfer, A., and Schewe, G., "Investigation of an Oscillating Supercritical 2D Wing Section in a Transonic Flow," AIAA Paper 99-0653, January 1999.

[24] Perko, L., *Differential Equations and Dynamical Systems*, Springer-Verlag, New York, NY, 1991.

[25] Farkas, M., *Periodic Motions*, Springer-Verlag, New York, NY., 1994.

COPYRIGHT STATEMENT